Studies of Liquid−Liquid Demixing of Polystyrene Solutions Using Dynamic Light Scattering. Nucleation and Droplet Growth from Dilute Solution

Jerzy Szydlowski† and W. Alexander Van Hook*

Chemistry Department, University of Tennessee, Knoxville, Tennessee 37996

Received December 5, 1997; Revised Manuscript Received March 12, 1998

ABSTRACT: Dynamic light scattering (DLS) measurements of liquid−liquid demixing from dilute polystyrene (PS)/cyclohexane and PS/methylcyclohexane solutions are described. Phase transitions were induced by temperature quenches into the metastable region and beyond using concentrations low enough to ensure liquid−liquid demixing by a nucleation growth (NG) mechanism. In a companion paper the NG results are compared with demixing studies at higher concentration, where the mechanism is spinodal decomposition (SD), and with DLS measurements in a good solvent. The present measurements employed polystyrenes of low or medium molecular weight, $M_{w,1} = 30\,000$, $\rho_1 = M_w/M_n = 1.05$, $M_{w,2} = 90\,000$, $\rho_2 = 1.04$ and $M_{w,3} = 400\,000$, $\rho_3 = 1.05$. In the NG region DLS measurements yield well-behaved correlation lengths for quenches well into the metastable region, but that pattern ends in the immediate vicinity of the cloudpoint where it splits to a bimodal distribution. The larger (slow) component is associated with the nucleation and growth of droplets of the precipitating phase. The rate of growth of the slow component was measured for the M_w 400 000 sample but growth was too rapid to follow at the lower M_w's. The splitting process is sensitive to both quench depth and quench rate. (At higher concentrations where liquid−liquid demixing is via an SD mechanism no splitting is observed. Instead, one finds well-behaved monomodal DLS correlograms which show exponentially increasing intensity and correlation length as the cloudpoint is approached.)

1. Introduction

Imre and Van Hook[1] have reviewed the thermodynamics of liquid−liquid demixing of solutions of polystyrene (PS) in various solvents including work from this laboratory in acetone, methylcyclopentane, propionitrile, and methylcyclohexane. Those studies include temperature or pressure quenches into the upper (UCS) or lower (LCS) two-phase consolute regions where phase separation occurs. Debye analysis[2] of the scattering data was used to define cloud and spinodal loci, and the results interpreted with a mean-field algorithim[3] combining Ratsch−Kehlen[4] continuous thermodynamic Flory−Huggins solution theory with the Bigeleisen−VanHook−Wolfsberg[5] formalism of condensed phase isotope effects. This approach has been used to define expressions which correlate the demixing diagrams with solvent quality, molecular weight, pressure, and other variables.[1] We now turn attention to studies of the mechanism of precipitation, using dynamic light scattering (DLS) to compare those parts of the phase diagrams where demixing is driven by nucleation and growth (NG, this paper), with demixing at higher concentration which follows spinodal decomposition−percolation, SD/P, and with DLS in homogeneous solutions.[6] Our objective is to clarify the distinction in kind between NG and SD/P by examining the details of DLS correlation lengths and intensities prior to and during phase transitions induced by temperature quenches. We plan to broaden the approach later by inducing transitions with pressure quenches and still later by continuously changing concentration, isotope label, or solvent quality to induce precipitation. DLS is a useful tool for comparisons between NG and SD/P precipitation and between temperature, pressure, and concentration quench induced transitions, as it directly interrogates the characteristic distance parameter which defines the concentration fluctuations ultimately leading to macroscopic phase separation. To anticipate, the experiments described in this paper and its companion,[6] while in reasonable accord with currently accepted ideas of NG and SD/P precipitation, clarify certain of the details of that interpretation, including (for NG precipitation) the kinetic dependence of nucleii development on quench depth and induction time, and the q-dependence of the DLS signal in the metastable region.

During the discussion it will be useful to refer to diagrams which correlate the free energy/concentration surface, $(G_{mix}, \psi)_\tau$, with the demixing phase diagram, (τ, ψ), using appropriate projections (τ represents an externally controlled variable, for example temperature, pressure, average chain length, etc., and ψ is concentration). Figure 1 shows demixing from a solution exhibiting upper consolute (UCS)/lower consolute(LCS) behavior. The heavy lines labeled "cx", "cp", and "sp" refer to coexistence, cloudpoint, and spinodal loci, respectively. At the ends of the tie lines connecting solutions in equilibrium on either of the coexistence curves (bb′ or mm′, for example) the partial molar free energies (chemical potentials) of each component in each phase are equal (α = solvent-rich phase, β = polymer-rich phase, 1 = solvent, and 2 = polymer, so $\mu_1^\alpha = \mu_1^\beta$ and $\mu_2^\alpha = \mu_2^\beta$, but generally $\mu_1^\alpha \neq \mu_2^\alpha$ and $\mu_1^\beta \neq \mu_2^\beta$). The spinodal is the locus of points of inflection, $\partial^2 G_{mix}/\partial\psi^2 = 0$. A system which lies inside either of the spinodals is absolutely unstable with respect to phase separation, $\partial^2 G_{mix}/\partial\psi^2 < 0$, and a solution quenched into this region, for example from point A to point B, Figure 1, spontane-

* To whom correspondence should be addressed.
† On leave at the University of Tennessee 1995−1996. Permanent address: Chemistry Department, University of Warsaw, Zwirki i Wigury 101, 02-089 Warsaw, Poland.

S0024-9297(97)01776-2 CCC: $15.00
Published on Web 04/23/1998

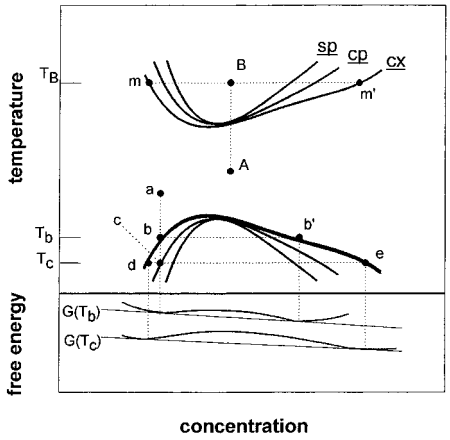

Figure 1. Relation between the $(G(T), \psi)$ surface at several temperatures and the phase diagram for liquid−liquid precipitation (schematic). $G(T)$ is the total free energy of the mixture and ψ the segment fraction polymer. The subscripts refer to the temperatures marked on the coexistence surface. The bottom part of the figure shows $(G(T), \psi)$ projections at T_b and T_c. The upper part shows the liquid−liquid demixing diagram in (T, ψ) space with upper consolute (UCS) and lower consolute (LCS) branches. $G(T)$ diagrams corresponding to the LCS branch (uppermost curves) are not shown to avoid clutter. *SP* = spinodal; *CP* = cloudpoint; *CX* = coexistence curve. See text for further discussion.

ously separates into daughter phases of compositions m and m′. This process of "spinodal decomposition" results in a characteristic "spinodal structure". After sufficient time (that is, in the later stages of the phase separation), spinodally decomposed mixtures consist of large irregularly shaped domains percolating throughout the two-phase matrix. Our present interest, however, is in the phase separation which occurs on quenching into the metastable area between the spinodal and coexistence surfaces (quench "a−b−c", Figure 1, for example). At a point like "c" in the metastable region the system meets the thermodynamic criterion[7] $(\partial^2 G_{mix}/\partial\psi^2 > 0)$. While phase separation is thermodynamically possible, it is not kinetically required even though the phase-separated system lies at a lower free energy than the homogeneous mixture. This implies the possibility of quenching from the one-phase homogeneous region, through the coexistence surface and the metastable region, into the area inside the spinodal surface, where, once reached, the phase change is spontaneously and immediately initiated (as in the quench labeled "AB"in Figure 1. Phase transitions in the metastable region may on the other hand be kinetically delayed, but once begun are driven to completion (because ΔG_{tot}(transition) < 0). They are usually recognized by the onset of turbidity at more or less reproducible (τ, ψ) loci, and this defines the cloudpoint. Clearly cloudpoints can lie no closer to the homogeneous region than the coexistence surface "cx", nor no further than the spinodal "sp". Metastable phase separation follows a nucleation/growth mechanism. For shallow enough quenches, for example the one labeled "a−b−c" in Figure 1, this results in a two-phase structure (microdroplets of dispersed minority phase) different in character from spinodally decomposed mixtures.

A good deal of theoretical and experimental interest in the kinetics and mechanism of phase separation in polymer solutions, particularly polymer blends,[8−13] has been biased toward studies of the early stages of demixing. Blend studies are useful because many phenomena of interest are diffusion controlled and occur too rapidly for experimental convenience in low viscosity solutions. Even so, some studies of nucleation−growth and demixing kinetics have been reported for polymer/solvent[14,17] and small molecule solutions.[18,19] The references, not exhaustive, are sufficient for access to the literature.

1.1. Precipitation in the Nucleation/Growth Region. Returning to Figure 1 consider a solvent-rich off-critical quench in the temperature domain ($\tau = T$), which starts in the homogeneous region at "a", is carried through the coexistence surface at "b", and into the metastable region, finally arriving at the cloudpoint, "c", where nucleation followed by growth, NG, intervenes. The cloudpoint is kinetically and not thermodynamically defined, and its precise location may depend on the rate of quench, the time of waiting for NG to develop after the quench, on wall effects, impurities, and other variables. Thus the cloudpoint may be operationally defined by the time scale of the experiment, i.e. the waiting time after quench in "step-quench" experiments, or the quench rate itself for "continuous-quench" experiments.

Now consider NG initiated at the cloudpoint ("c" in Figure 1). Before precipitation the reduced free energy of the metastable parent phase located at "c" is $G_c/(RT_{c,cp}) = (G_b/RT_{b,cx}) + (\Delta H_b/RT_{b,cx})((T_{b,cx} - T_{c,cp})/T_{c,cp})$, neglecting higher order terms which account for heat capacity effects. The free energy difference which expresses the extent of metastability can also be determined by integrating along the concentration axis, $G_c/(RT_{c,cp}) = (G_d/RT_{d,cx}) + (\partial G_{tot}/\partial\psi)(\psi_c - \psi_d)$. At equilibrium the coexisting phases, shown at points "d" and "e" (Figure 1), are present in relative amounts given by the tie line rule, [κ = (polymer rich/polymer poor) = $(\psi_c - \psi_d)/(\psi_e - \psi_c)$]. The free energy of the phase separated system is $G_{sepd}/(RT_{d,cp}) = (1/(1+\kappa))(G_e/(RT_{d,cp})) + (\kappa/(1+\kappa))(G_d/(RT_{d,cp}))$. The reduced free energy difference driving the phase change, $\Delta G/(RT_{cp}) = (G_{sepd} - G_c)/(RT_{d,cp})$, is negative, and this accounts for the splitting from one to two phases.

The limit of metastability, i.e. the cloudpoint temperature, is calculated in first-order classical theories by taking the surface free energy of the separating phase into account, $G_e = G_e^{blk} + 2\sigma/r$, where G_e^{blk} refers to the bulk phase free energy, σ denotes the interfacial tension, and r is the radius of the initially separating microdroplets.[20,21] The surface term raises the free energy and accounts for metastability in the unseparated parent solution. In first order theory the cloudpoint is specified by solutions to the equation, $\Delta G = (G_{sepd} - G_c) = 2\sigma/r$, but this approach sometimes predicts unrealistically large numbers of molecules and/or metastable excess free energies in the critical nucleus. Bowers, Eli, and Noyes[22] have recently investigated alternative unstable structures ("blobs") which do not have well-defined interfaces; the effective interfacial surface tension defining nucleation in the blob model is low. Blobs may exist transiently as precursors of the precipitating phase, and this circumvents the necessity of postulating a large metastable excess free energy of formation.

Pecora[23] and Brown,[24] among others, have reviewed the use of dynamic light scattering to investigate certain of the length scales characterizing precipitation from polymer solutions. At the low concentration limit (isolated polymer chain) the DLS correlation length, ξ_{DLS}

$= \xi$, reduces to the hydrodynamic radius, $\xi^0 = r_h$. Thus one expects the simplest possible DLS pattern of an about-to-precipitate or precipitating solution in the NG region to show a bimodal distribution of DLS ξ's, one component scaling characteristically with the size of the dissolved isolated polymer chains, the second scaling with the size of the precipitating polymer-rich nuclii. Later in this paper we present data supporting that point of view. We close this section by noting that NG precipitation is observed only in dilute solutions, i.e, $0 < c/c^* < \sim 0.5$, where c^* is the overlap concentration, $c^* = 3M_w/(4\pi N_{Av} r_g 3)$, r_g is the radius of gyration, and N_{av} is Avogadro's number.

1.2. The Transition from NG to SD/P Precipitation. Tomlins and Higgins[13] discuss demixing using a diagram similar to Figure 1 except that they insert an additional line which they call the "percolation threshold (PT)". PT, like the cloudpoint locus CP, lies somewhere between the coexistence and spinodal loci, CX and SP. Between PT and CX, droplets or clusters of precipitate are considered to be isolated, and below PT they are interconnected. According to the authors[13] the "microdrop" structure can only form between the cloudpoint and percolation threshold in quench experiments, and once formed should not dissolve until the τ variable once again passes through the coexistence locus into the homogeneous region, (i.e., on reversing the sign of the quench). Below the percolation threshold the clusters are assumed to percolate or ramify throughout the matrix. This should be reflected in the light scattering properties of the mixture. In contrast to the situation for NG, no abrupt or discontinuous shifts in scattering intensity or the distribution of correlation lengths are expected as the PT boundary is approached and crossed. Rather, one finds both scattering intensity and correlation length logarithmically scale toward infinity as the transition is approached.[6] Thus, there seems to be little or no experimental distinction between structures characterizing precipitation in the PT region and spinodal decomposition, although apparently Tomlins and Higgins would use PT to describe precipitation in the upper parts of the metastable region, reserving the term SD for quenches which actually extend into the spinodal region. As concentration increases the metastable gap narrows, cp approaches sp, and SD/PT (SD/P) becomes the more likely mechanism for liquid−liquid demixing. We suggest that the transition between NG and SD/P precipitation, not sharp, can be operationally defined using the temperature dependence of the DLS correlation length, which shows a simple linear behavior on quenching to the region of CP in the NG region, but scales exponentially for SD/P precipitation. We observe the change from NG to SD/P well below overlap concentrations.

2. Experimental Section

2.1. Materials and Sample Preparation. Polystyrene samples of low polydispersity were purchased from Scientific Polymer Products or Pressure Chemical Company and are further specified in Table 1. Reagent grade cyclohexane (CH) and methylcyclohexane (MCH) were purchased from Aldrich Chemical and used as received except for drying over molecular sieve. Solutions were prepared gravimetrically and stored in well capped vials. They were clarified immediately before use by making multiple passes through Millipore poly(tetrafluoroethylene) 0.2 μm (Alltech or Whatman) filters into thoroughly clean dust-free cylindrical Pyrex scattering cells of various dimensions. LS data improve markedly in quality as cell diameter increases and most of the present data were gathered using cells with $d \sim 12$ mm or greater.

Table 1. Properties of Polystyrene/Methylcyclohexane Solutions

M_w	3×10^4	9×10^4	40×10^4
symbol	PS30K	PS90K	PS400K
M_w/M_n[a]	1.03	1.04	1.06
r_h/nm[b]	(3.4)	(6.0)	(13.2)
r_g/nm[c]	(4.2)	(7.5)	(16.5)
c^*/(mg·ml)[d]	160	85	35
T_{crit}	302	320	333

[a] Manufacturer's specification. [b] Using $(r_h/r_g)_{MCH} = (r_h/r_g)_{CH} = 0.80$.[29] [c] Calculated by correlating known r_g values[29] with solvent quality index R_{12}.[1] [d] $c^* = 3M_w/(4\pi N_{av} r_g^3)$. [e] Reference 1.

2.2. Static and Dynamic Light Scattering. The light scattering measurements were made using a Bookhaven Instruments Corporation package which includes a computer-controlled BI-200SM goniometer, BI-9025AT correlator and signal processor, EMI B2FBK/RMI photomultiplier for photon counting, Spectraphysics model 127 50 mW He−Ne laser, and an associated software package for analysis of static light scattering (SLS) and dynamic light scattering (DLS) data including single and double exponential, CUMULANT and CONTIN data analysis packages.[25] The instrumentation package provides SLS and DLS data of useful quality for $(15 < \theta/\text{deg} < 155)$. We also qualitatively observed SLS at lower angle $(\sim 3 < \theta/\text{deg} < \sim 8)$ by projecting the transmitted beam onto a screen on the back wall of the instrument enclosure. In this way one can observe the development and decay of characteristic scattering rings (halos) correlating the observations with SLS or DLS measurements at higher angle.

For scattering measurements the sample cells were centered in a toluene-filled thermostated bath (~0.01 K) for refractive index matching. The toluene bath is slaved to an external circulator (Model 704 Hart Scientific, ~0.001 K). For temperature quenches, the master thermostat is manually adjusted to provide the desired heating or cooling rate. The precision of thermostating at the scattering cell has deteriorated about an order of magnitude from the master bath but, nonetheless, remains adequate for our purposes.

2.3. Experimental Determination of Coexistence and Cloudpoints. Cloudpoint loci are straightforwardly defined by characteristic changes in the DLS or SLS scattering intensities as described in later sections. We used several different methods to determine coexistence points. The most straightforward was to determine the dissolution temperature of clouded but unsettled suspensions by monitoring the abrupt dimunition of LS intensity, which occurs on passing through the coexistence point back into the homogeneous region. This is conveniently done by reversing the sign of the temperature quench before appreciable sedimentation occurs in the partially phase separated mixture. In the second method, cloud and coexistence points were observed in capillary scattering cells on unclarified samples. Unclarified solutions and/or solutions in small containers (where wall effects are much more important) are less likely to withstand quenches beyond "cx" and into the metastable region. Finally for experiments in the (T,ψ) domain we sometimes estimated $\delta_T(\text{max}) = (T_{coex} - T_{cloud})$ using an empirical relation suggested by Howland, Wong, and Knobler.[18]

2.4. Viscosity and Surface Tension. Viscosities, densities, and surface tensions of the CH, MCH and DEO solvents, and selected polymer-poor and polymer-rich solutions, were obtained from standard sources or measured using Ostwald capillary flow, pycnometry, or capillary rise.

3. Results and Discussion

3.1. General Remarks. The present experiments measure DLS in the vicinity of cloudpoints. DLS correlation lengths, ξ_e, show pronounced change in character as concentration increases from $c/c^* \ll 1$ to $c > \sim c^*/2$; $c^* = 3M_w/(4\pi N_{Av} r_g^3)$ is the overlap concentra-

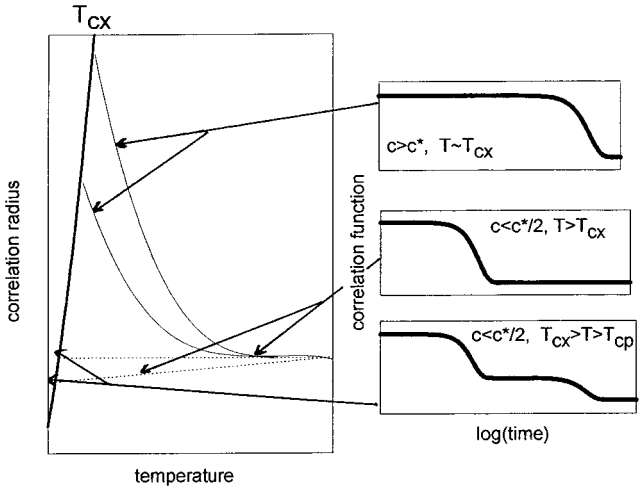

Figure 2. Behavior of the DLS (hydrodynamic) correlation radius, ξ, as a function of T in the vicinity of precipitation at various concentrations. DLS correlograms corresponding to different parts of the diagram are shown in the inserts. For $T \gg T_{cp}$ and $c < \sim c^*/2$, $\xi \sim r_h$ with $\partial\xi/\partial T > 0$ and small (lower two curves). The corresponding correlogram (middle insert) is a well-behaved monomodal single exponential, which discontinuously splits at low enough temperature (just prior to the onset of precipitation) to bimodal (bottom insert). For $c > \sim c^*/2$, however, $\partial\xi/\partial T < 0$, and it smoothly increases in magnitude as T is decreased, exponentially diverging as T_{cp} is approached (upper two curves). No splitting is observed. The correlogram (upper insert) maintains a well-behaved monomodal single-exponential all the way to the phase transition and the process can be described using logarithmic scaling relations.[6] The light dotted and solid lines refer to different concentrations, increasing from bottom to top.

tion. Typical behavior during quenches to T_{cp} and beyond are schematically shown in Figure 2. The NG and SD/PT regions are compared. The discussion is based on our observations of PS/400K-CH and PS/30K-MCH solutions in the NG (present paper) and SD/PT regimes,[6] which are consistent with other reports in the literature *(vide infra).* For $c < \sim c^*/2$ and $T > T_{cx}$ the autocorrelation function a is well-behaved single exponential at all concentrations leading to NG precipitation. Correlation radii, ξ, remain close to the low concentration limit. They decrease slowly and continuously with T as the coexistence surface is approached and then cross into the metastable region, $(\partial\xi/\partial T)_{c<c^*/2} > 0$. Slightly above T_{cp} the autocorrelation function, monoexponential to this point, abruptly splits. As time passes (or quench depth increases) the new and slower (larger ξ_2) component increases in intensity at the expense of the original component, $I(\xi_1)$, which gradually subsides until it is lost in the background. The details of the splitting process depend sensitively on molecular weight, quench depth, waiting time, concentration, *etc.*, and are discussed in the following section. Both slow and fast modes are diffusive for these dilute, but about to precipitate, solutions. We emphasize that the change in the autocorrelation function from that characterizing a single well-behaved fast mode (associated with the isolated but solvated polymer) to the fast-mode/slow-mode couple (which we assign to the process "isolated polymer = subcritical or critical nucleus") is discontinuous. Precipitation in the NG region cannot be described using logarithmic scaling.

As concentration increases the shape of (T, ξ) changes. Both scattering intensity and correlation length increase with quench depth. $(\partial\xi_1/\partial T)$ which is small and positive for $c \ll c^*$, changes sign, and in the semidilute and high

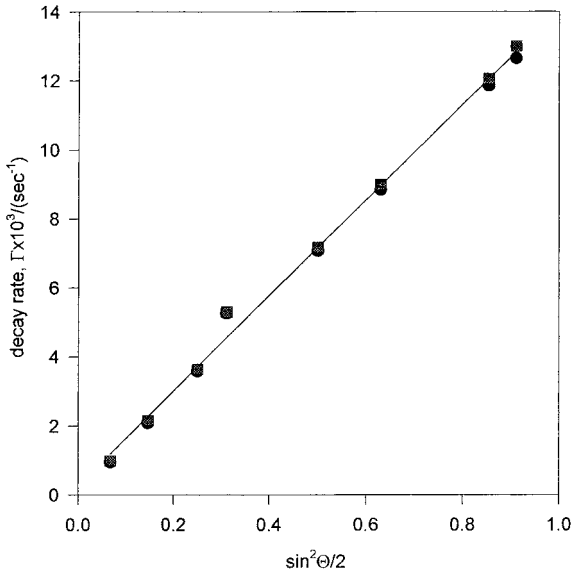

Figure 3. Angle dependence of the decay rate for PS-400K-CH solution, 0.13 wt %, at 23.9 °C. The linear dependence of the decay of the argument of the autocorrelation function, Γ vs $\sin^2(\theta/2)$, establishes data quality and demonstrates that corrections for multiple scattering may be neglected. Recall $g_1(t) = B \exp(-\Gamma t)$; see text.

concentration regions ($c/c^* > \sim 0.5$) exponentially increases in magnitude as temperature falls to T_{cx}, $(\partial\xi/\partial T)_{c>c^*} < 0$. In this region the (T, ξ) curves follow logarithmic scaling, $\xi \sim At^{\nu}$, t is a reduced temperature, $t = |(T - T_{cr})/T_{cr}|$, A is a fitting parameter, and ν a scaling exponent. The autocorrelation functions maintain well-behaved single exponential character, at least until the intensity becomes so large that multiple scattering intervenes. We associate this region with a precipitation mechanism different from NG and, following remarks in the previous section, label it (SD/P). DLS patterns in this region are strictly reminiscent of those seen on quenching directly into the unstable region at or near the critical concentration. It seems reasonable to associate the change from NG to SD/P with that concentration (or range of concentrations) where $\partial\xi/\partial T \sim 0$. We reemphasize that for these higher concentrations, $\sim c^*/2 < c < c_{cr}$, the DLS data evidence no sign of a discontinuous NG mechanism of precipitation even though the temperature quenches inducing precipitation were halted well before the spinodal locus was crossed. Further discussion of precipitation in the SD/P region is reserved to a later paper.[6]

At concentrations well above critical and into the entanglement region the autocorrelation functions deteriorate further, splitting into a fast diffusive mode (which is concentration and temperature-dependent according to logarithmic scaling) and a slow nondiffusive mode. The slow mode has been assigned by Brown and co-workers[24,26] to the formation of a highly entangled, high concentration incipient gel state.

3.2. Precipitation Experiments in the NG Region. We carried out a variety of quench experiments, mostly on samples with $M_w = 3 \times 10^4$, 9×10^4, or 4×10^5. Both continuous and step-quench techniques were employed. Most often the early stages of phase separation were studied using DLS at one or more angles to test data quality (for an example see Figure 3), recording the dependence of the autocorrelation function on quench depth and/or time of waiting at a given depth. Results are summarized in this and following sections.

We have found graphical representations of the data to be especially informative for these experiments and have chosen to report most of our observations graphically.

DLS results are usefully represented either in terms of diffusion constants, D, or hydrodynamic correlation radii, ξ, of the different species in the mixture, as convenient. These parameters are deduced from the raw DLS data by cumulant analysis, or CONTIN.[25,27] For monodisperse small particles the electric field correlation function (most directly measured in the DLS technique) is of the form, $g_1(t) = B \exp(-\Gamma t)$, and this yields the translational diffusion constant, D, using $D = \Gamma/q^2$. B is a constant which depends on the optical setup of the experiment. The DLS correlation radius, ξ_e, follows via the Stokes−Einstein relation, $\xi = k_B T/(6\pi\eta_o D)$, where k_B is the Boltzmann constant and η_o is the solvent viscosity. The zero concentration limit of ξ defines the hydrodynamic radius, $\lim_{c=0}(\xi) = r_h$, and $\lim_{c=0}(D) = D_0$ which is the single particle diffusion constant. Multiexponential decays are dealt with by applying higher order or CONTIN fits to the logarithmic correlation function. The process defines apparent diffusion constants and apparent correlation radii, which at a given temperature may be both q and c dependent.

In the homogeneous region, i.e., well above the cloud and coexistence surfaces, the scattering intensity is low. DLS correlation radii, ξ, are of reasonable magnitude but show marked temperature and concentration dependences; for examples, see the figures in this paper, especially Figure 2. In this region, far from the phase transition, the ξ values are independent of scattering angle (Figure 3). Although the figure shows only one example, the q-dependence was in fact carefully checked for all concentrations and temperatures. The observation is important. It demonstrates that corrections for multiple scattering are not necessary, and establishes the ξ values (or correlation times from which they are derived) as meaningful physical quantities. Very close to precipitation, however (i.e., after formation of the bimodal DLS pattern which occurs well inside the metastable boundary), the decay of scattering intensity with angle becomes very strong, orders of magnitude larger than would be predicted from first order theory for scattering from centers smaller than $\sim^1/_{20}\,\lambda$. Such intensity effects are a consequence of interference (scattered intensities from different parts of the correlated region are out of phase; this damps the intensity for measurements at large angle).[28]

We now turn to the description of off-critical quench experiments in the NG region. Under these conditions well-defined hydrodynamic radii which characterize the isolated polymer are obtained from the DLS data (∼3.6 nm for PS = 30K, ∼6 nm for PS = 90K, and ∼13 nm for PS = 400K) and can be usefully compared with r_h and ξ values in good solvents.[29] For NG quenches we find a characteristic temperature or narrow range of temperatures near T_{cp} where DLS based ξ's discontinuously split from a single peak narrowly centered at ∼3.6 nm for PS = 30K, ∼13 nm for PS = 400K, into a doublet ($\xi_{e,1}$ = 3.5 nm, $\xi_{e,2}$ ∼ 150 nm for PS = 30K; $\xi_{e,1}$ = 13 nm, $\xi_{e,2}$ ∼ 150−220 nm for PS = 400K), but there are important qualitative differences between the solutions which are described beginning in the next paragraph but one.

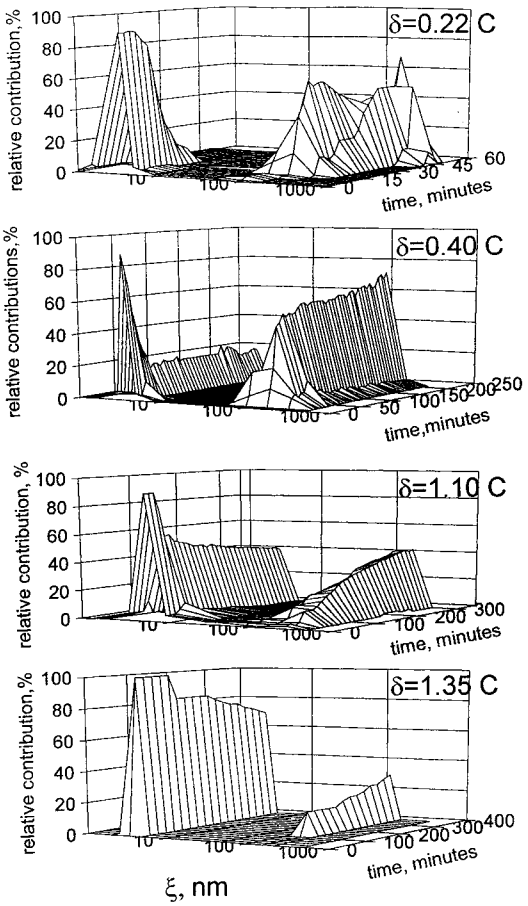

Figure 4. Early stage NG development for PS30K/MCH, 1.0 wt % and $2\theta = 15°$, at several quench depths, $T_q = T_{cp} + \delta$. From top to bottom (a) $\delta = 0.22$, (b) $\delta = 0.40$, (c) $\delta = 1.10$, and (d) $\delta = 1.35$ °C. For this solution $T_{cx} = 24.4$ °C and $T_{vcp} = 22.90$ °C. The time evolution of the diagrams is discussed in the text.

During all except the earliest studies we made qualitative observations of low angle SLS simultaneously with the DLS measurements by allowing the transmitted beam to fall on a screen at the rear of the instrument housing. At the point of initial splitting from the ξ_1 to the ξ_1/ξ_2 structures a characteristic low angle ring pattern appears which grows in intensity as ξ_2 develops. We now discuss qualitative differences in DLS patterns near T_{cp} for PS-30K/MCH and PS-400K/CH solutions in the NG region. The solvents are analogous and were varied only to force transitions to a convenient temperature.

3.3. Step Quenches in PS-30K/MCH Solutions. The behavior of PS solutions in the near vicinity of NG precipitation is illustrated by the series of quench experiments shown in Figure 4. In these experiments a 1 wt % PS-30K/MCH solution was quenched from 25 °C to T_q over a period of some minutes or so and then held at that temperature for many hours, periodically recording the DLS spectrum at $\theta = 15°$. T_q lies in the metastable region, ($T_{cx} > T_q > T_{cp}$). We define $\delta = T_q - T_{cp}$ and show DLS patterns as a function of time for $\delta = 0.22$, 0.40, 1.10, and 1.35 °C in Figure 4. To begin, consider the general behavior illustrated in Figure 4a, $\delta = 0.22$ °C. For $\delta > 0$ as the quench nears T_{cp}, the DLS correlogram for PS-30K abruptly splits into two stable forms after some delay. Close to T_{cp} the smaller (faster) component (∼3.5 nm) lies only slightly below its high temperature value (homogeneous region). The second and slower component appears almost discon-

tinuously over a time interval which is short compared to the rate of temperature change, or to the time required for a single DLS measurement, and we were unable to observe the growth kinetics defining the initial formation of the $\xi_{e,2}$ structure. Figure 4a shows the DLS structure after a step-quench which was halted in the metastable region 0.22 K above T_{cp} (and 1.3 K below T_{cx}). The ξ_2 structure appears after a brief delay. One notes an increase in relative intensity, $I(\xi_2)/I(\xi_1)$, with time but no significant shift in the values of either ξ_1 or ξ_2. After long enough time the bulk of the intensity is associated with ξ_2. Scattering intensity is exquisitely sensitive to particle size and these data are not precise enough to permit calculation of the relative concentrations of the ξ_1 and ξ_2 structures from the intensity data.

The development of the ξ_2 structure is very sensitive to quench depth as may be seen by comparing parts a−d Figure 4. At $\delta = T_q - T_{cp} = 1.35$ K (Figure 4d) the first traces of $\xi_{e,2}$ at a scattering angle of 15° appear after a delay of about 120 min. The DLS signal corresponding to ξ_2 grows in gradually. After 6 h the $\xi_{1,15°}$ and $\xi_{2,15°}$ signals are roughly commensurate in intensity, but even after 6 h only the smaller (ξ_1) component can be seen at 90°, and the low angle SLS conical ring pattern projected at the rear of the instrument housing is barely beginning to develop. After 20 h there has been no change in the ξ_2/ξ_1 distribution (∼3.5 and ∼160 nm), but the relative intensity of ξ_2 has increased to about 40%.

Compare the behavior above, $\delta = 1.35$ K quench with that for $\delta = 1.1$ K (Figure 4c). The first traces of $\xi_{e,2}$ appear after only 40 min at 15° scattering angle, after 4 h its contribution has reached ∼50% but then shows essentially no change for 23 h. These trends continue as δ falls toward zero (parts b and a of Figure 4), although the ξ_1/ξ_2 distribution, still bimodal, broadens a bit for δ small. For $\delta = 0.22$ K, ξ_2, now centered at 160 nm, has measurable components at 89 and 280 nm. The signal first appears after 13 min. At 32 min its relative intensity has increased to 93% and dominates, (however the DLS signal at 90° is still monomodal (ξ_1 = 3.5 nm, relative intensity ∼100%), at this angle the DLS measurements offer no hint of the approaching precipitation event).

3.4. Visual Observations near the Cloudpoint. Near T_{cp} it is useful to couple DLS with visual observation of the low angle SLS pattern projected on the back wall of the instrument enclosure. Close to T_{cp} the bright central spot which characterizes the transmitted beam in the homogeneous region becomes surrounded by a set of diffuse but well-defined halos which appear at about the time the 90° DLS pattern splits from the ξ_1 to the ξ_2/ξ_1 structure. As the transition proceeds (via quenching to or slightly below T_{cp}), these grow in number (spacing between the rings decreases) and intensity. Still later the ring pattern becomes grainy, which graininess becomes more noticeable with time, and the circular pattern loses definition as the polymer-rich phase begins to settle. The diminution of the ring structure is dynamic in character; different regions show marked intensity fluctuations on a time scale which, we estimate, is on the order of tens *per* second. With temperature continuing to fall the entire pattern eventually fades into smooth graininess, transmitted intensity continues to decrease, and finally the scattering pattern is lost entirely. The earlier part of this process is approximately reversible. When the sign of the temperature change is reversed, the grainy pattern reappears, rings form, etc., but the eventual loss of the rings as precipitate redissolves is temporally less sharp than was the initial appearance of the ring pattern. This is probably because the initial size distribution at T_{cp} is sharply bimodal (see below), broadens as the precipitate ripens, but does not resharpen as the coexistence surface is approached from below.

The low-angle SLS pattern observed on quenching to T_{cp} first develops at the point where DLS intensity is increasing markedly, i.e., just prior to and during precipitation. That initial increase in intensity is dramatically angle dependent, but in comparing the DLS and SLS patterns one should correct for the fact that human visual acuity (in this case used to observe the low-angle SLS pattern) is orders of magnitude less than PMT sensitivity used to measure DLS. For PS-400K/CH solutions the initial appearance of the SLS ring pattern occurs well before we observe (30°) DLS splitting to the bimodal $\xi_{e,1}/\xi_{e,2}$ pattern. In fact SLS rings for these solutions are seen some 0.2−1 K, or so, above T_{cp}. For these higher M_w samples the development of the ξ_2 mode is slower than for PS-30K/CH, and we were able to measure growth curves by halting the quench at an appropriate temperature close to T_{cp} (vide infra). For PS-30K/MCH solutions SLS rings did not appear until $T \sim T_{cp}$; however, the splitting to the DLS ξ_2/ξ_1 structure was observed much earlier (i.e. well above T_{cp}, see Figure 4).

3.5. Two Deep Quenches and a Continuous Quench. It is interesting to consider the effect of lowering temperature below T_{cp}. An example of an experiment in which the temperature is lowered to T_{cp} and then beyond, is shown in Figures 5 and 6 (PS-90K/CH, 3%, $T_{cp} = 18.05$). At 18 °C an appreciable contribution from ξ_2 (∼300−500 nm) appears. Its relative intensity grows in at the expense of $I(\xi_1)$ (∼15 nm), then decays when the sample is held at 17.75 °C for 30 min or more. We attribute this observation to the process of growth and settling of precipitating phase. Once this process is completed, the somewhat diluted solution now sits on the coexistence line. A second step quench to 17.00 °C results in rapid formation and growth of a new crop of polymer-rich precipitating phase, but as this grows in, and then then settles from solution, the ξ_1 (∼15 nm) mode again appears. At this end stage the remaining solution is appreciably solvent enriched. The observation of importance, again, is that in the NG region the precipitation process involves a pseudo-equilibrium between the members of a bimodal distribution of particle sizes so far as the polymer component is concerned. The DLS measurements give no indication whatsoever that intermediate-sized particles make any contribution to the structural properties of the solution.

It is interesting to compare the DLS patterns for precipitation of the 3% solution discussed above and in Figures 5 and 6 with the behavior of a more concentrated solution. Figures 7 and 8 reports on a more concentrated PS90K/CH solution, (6.6% PS, T_{cp}=18.75), quenched below its cloudpoint. The behavior is significantly different from the 3% solution. As T is lowered from ($T_{cp} + 4.25$) to T_{cp} there is a continuous growth in correlation length (from ∼28 to ∼89 nm), and although a splitting is observed at $T_{cp} \sim 18.75$, its characteristics are quite different from that seen at lower concentration. In the more concentrated case ξ_2 initially appears

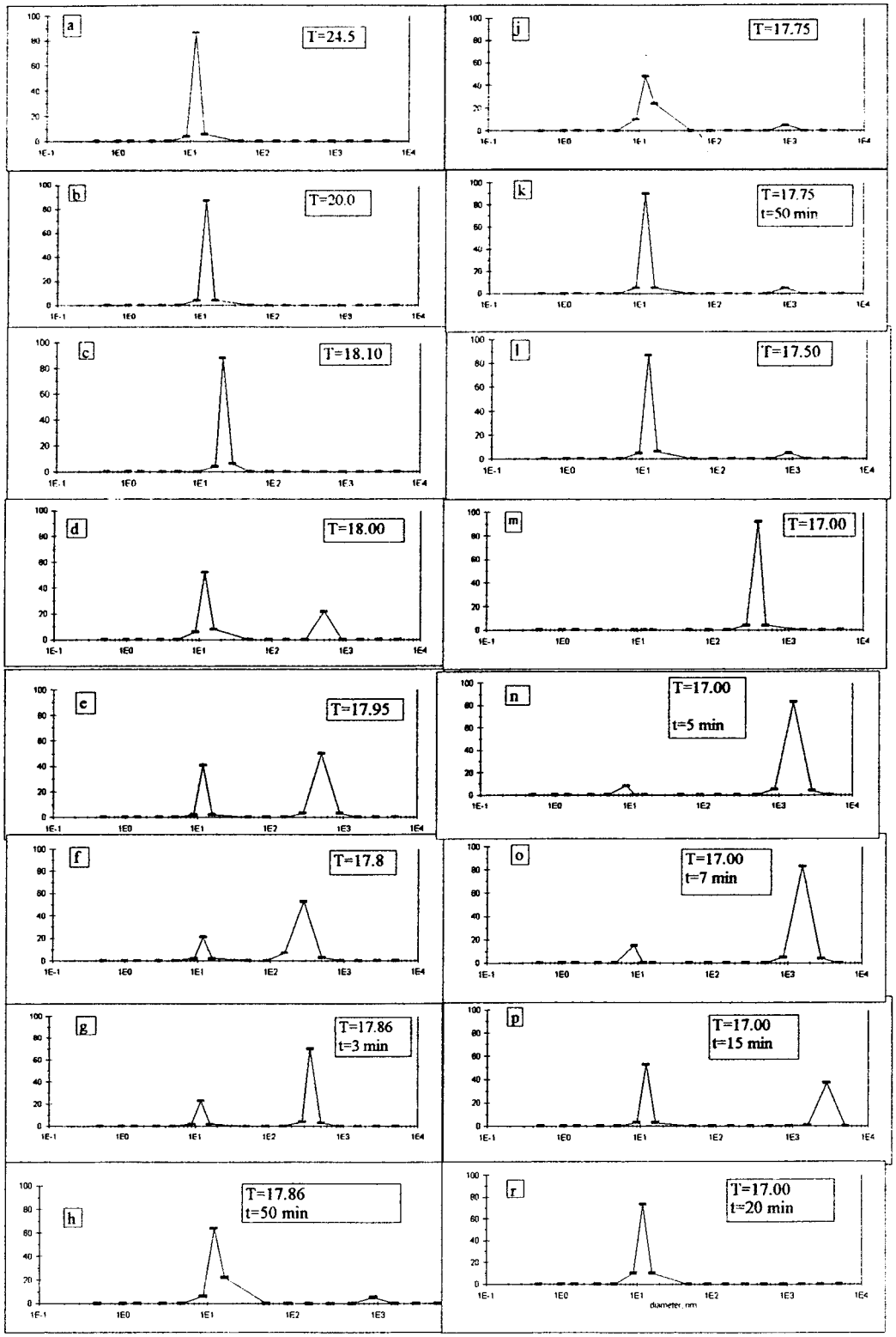

Figure 5. Nucleation and growth from a PS90K/CH 3 wt % solution during a series of step-quenches to T_{cp} and below at a 90° scattering angle. Relative contribution to intensity is plotted vs correlation radius at various temperatures. For this solution T_{cp} = 18.05 °C. In frames a through c little change is observed in the ξ_1 structure as the solution is lowered to the T_{cp}. Below that temperature the bimodal ξ_1/ξ_2 develops then diminishes as precipitation takes place at 17.86 °C, the solution being held at that temperature (h). After further lowering of the temperature to 17.00 °C (j to m) a second round of precipitation (n to r) ensues as the sample is held at 17.00 °C. At the end of the process the solvent-enriched solution is once again in the ξ_1 structure.

at a high value and as precipitation proceeds ξ_1 shifts down again toward lower values (for the more dilute solution, ξ_1 sits at approximately the same value throughout the quench). Recall that at even higher concentrations the DLS pattern does not split discontinuously into fast and slow modes as the transition is approached but rather maintains a single exponential character throughout which diverges as critical demixing is approached. The examples underscore the complexity of the concentration dependence of scattering in the poor solvent and about-to-precipitate regime. For both low and moderate concentrations (3.3 and 6.6% in

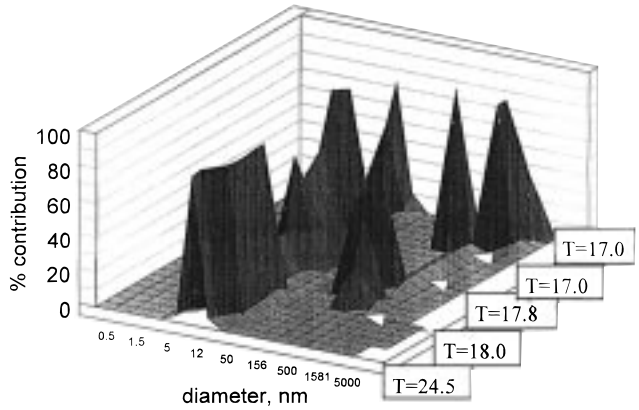

Figure 6. Three-dimensional representation of the data discussed in Figure 5.

the example under discussion) scattering intensity increases markedly as T_{cp} is approached. Figure 8 shows $1/I$ vs T for $T > T_{cp}$ (6.6% solution) which in the Debye interpretation leads to the prediction T(spinodal) $\sim$ 18.3 °C. The figure is representative of the behavior of most of the scattering data reported in this paper.

Figure 9 reports observations of a continuous quench for a dilute solution (from 19 to 12 °C for PS-90K/CH, 0.2%). Once again we see the expected features, although slowed because of the now very low concentration. The discontinuous splitting from the ξ_1 to ξ_1/ξ_2 pattern at T_{cp} is evident. The initial splitting, again, is followed by a slow growth in size and intensity of the precipitating particles, which in the present (low concentration) case remain suspended in solution over the time scale of the experiment.

3.6. Multiple Scattering. During the early stages of NG precipitation the distribution of ξ_1/ξ_2 values (still bimodal) is angle independent, and multiple scattering corrections remain unimportant. However, as the precipitating particles grow (at longer times or for $T < T_{cp}$), the decay of scattering intensity with angle becomes very strong. Multiple scattering and single particle interference effects come into play as the number and size of the $\xi_{e,2}$ particles increase, and the autocorrelation function distorts. The precipitation cannot be quantitatively interpreted in terms of physically meaningful ξ_2's. Even so, it is interesting to note that pseudo-correlation lengths, $\xi_2^{@}$, (i.e., those calculated from the observed autocorrelation functions with no concern for multiple scattering corrections), appear to be qualitatively the same as the properly evaluated ξ_2 parameters obtained from low-intensity DLS measurements during early stages of the preprecipitation or precipitation (i.e., in the absence of multiple scattering). Even though the angle dependence of the scattering intensity increases by orders of magnitude for T just below T_{cp}, the changes in the autocorrelation function are modest, it is relatively well-behaved. It is unfortunate that presently available software does not include corrections for multiple scattering and/or other interference effects. As a consequence, our discussion of high-intensity DLS at intermediate stage precipitations remains necessarily qualitative. (The situation improves for essentially opaque samples such as colloidal dispersions. Here very high multiple scattering permits application of diffuse wave spectroscopy.[30]) The onset of multiple scattering in the present solutions is most easily judged by visually observing ($\sim$90°) the laser beam as it passes through the solution. At the point where multiple scattering becomes important, it changes from a sharp well-defined beam to a diffuse cone.

3.7. Development and Persistence of the ξ_2 structure. Step quenches on PS400K/CH solutions: The structure associated with ξ_2 resists precipitation on a time scale of hours so long as temperature is not allowed to fall below the visual cloudpoint. Figure 10 illustrates a quench which ends 0.22 K above T_{cp} for a dilute PS400K/CH solution (0.13 wt %). The high dilution and low concentration combine to slow the induction time to first appearance, and the rate of development of the ξ_1/ξ_2 structure. That structure grows in according to well-defined kinetics discussed below and then decays as the precipitating particles settle from the beam. For these reason $I(\xi_1)$ displays a well-defined minimum which reflects the growth and decay of the ξ_2 structure.

The induction times and kinetics of the development of the $\xi_{e,2}$ feature are illustrated in Figure 11 for a series of eight quenches of PS400K/CH solutions (0.13%) over the range $0.05 < \delta < 0.34$, ($T_q = T_{cp} + \delta$). Under these conditions, DLS intensities measured at 90° are undetectably small. The present measurements refer to a scattering angle $2\theta = 30°$. The induction time, t(ind), for $\xi_{e,2}$ is defined as the time lapse from quench halt to first appearance of bimodality in the autocorrelation function. It is a sensitive function of the quench depth. In each case we started with a well-defined single-exponential autocorrelation function with $\xi_1 \sim 12-14$ nm and visually observed the appearance of low-angle SLS rings (vide supra) at the same time the system initially split into its bimodal form. Figure 11a shows for a quench ending just above T_{cp}, $T_q = T_{cp} + \delta$, $\delta =$ 0.05 K, that the induction time is too small to measure by the present technique, while for $\delta = 0.34$, it has increased to $\sim$4 h. Parts b and c of Figure 11 show the development of slow mode correlation radius, ξ_2, and intensity, $I(\xi_{e,2})$, both growth curves naturally offset by virtue of the induction periods. On the other hand the constants which describe the rate of increase of ξ_2 and $I(\xi_2)$ do not change much with δ. To present precision both rate processes are first order (see Figure 11 b,c). Intensity is a complicated function of particle size and number density.

For deep quenches ending below T_{cp} we were unable to obtain rate constants which quantitatively describe $\partial\xi_2/\partial t$ or $\partial I(\xi_2)/\partial t$ even for dilute solutions. In this region the growth is too rapid to follow by our technique. Also the measurements are complicated by multiple scattering which becomes important below T_{cp}. Qualitatively we observe that the autocorrelation functions change from monomodal to bimodal when the transition is first induced, then back to monomodal but now of large size (long time) as the precipitating particles grow in. The ratios $I(\xi_2)/I(\xi_1)$ do not scale with size alone and do not measure relative number densities in any simple fashion. We conclude that the geometric structure associated with ξ_2 is most likely no larger than the critical nucleus required for precipitation but immediately caution that no evidence has been presented which allows one to assume that the ξ_1 and ξ_2 structures are distinguished from each other by well-defined surfaces of the kind assumed in classical nucleation theory.[22]

3.8. Literature Comparison: DEO Solutions. It is interesting to compare these observations with other reports of bimodal ξ distributions in the vicinity of the cloudpoint. Sato, Kuwahara, and Kubota[14] performed

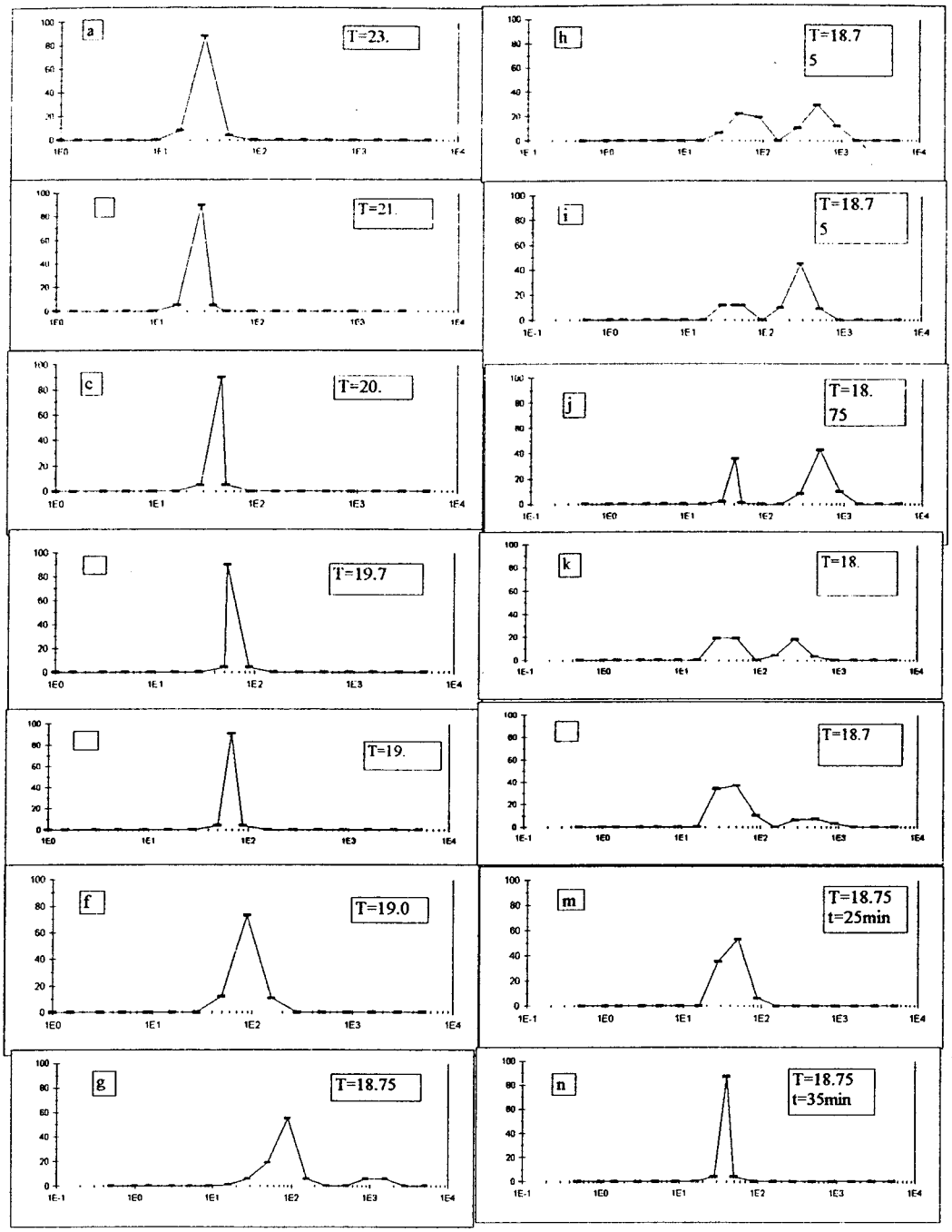

Figure 7. Nucleation and growth from a PS90K/CH 6.6 wt % solution during a series of step-quenches below T_{cp} at a 90° scattering angle. Relative contribution to intensity is plotted vs correlation radius at various temperatures. For this solution $T_{cp} = 18.75$ °C. Differences in the time evolution of DLS signal with extent of precipitation for the 3% (Figures 5 and 6) and 6.6% solutions (this figure) are discussed in the text. Most importantly, notice the values of the correlation radii, ξ_1 and ξ_2, vary with extent of precipitation for the 6.6% solution, but are more nearly invariant for the more dilute solution (Figures 5 and 6).

quench experiments for PS-600K/diethyl oxalate (DEO) solutions. PS and DEO are nearly isopycnic and the coexisting phases have nearly the same density. Sedimentation and ripening processes which depend on sedimentation are slowed. Experiments were carried out on very dilute solutions (0.04 wt % PS) and the observations are interestingly different from the ones reported in this paper. According to Sato et al. the DLS correlation radii of the large particles, once they form, increase logarithmically with time according to a two-stage process: (a) an initial phase where $\xi_2 \sim t^1$, $I(0,t) \sim t$,[6] and $N(t) \sim t^0$ with ξ_2 a strong function of quench depth and (b) a later stage with $\xi_2 \sim t^{1/3}$, $I(0,t) \sim t^1$, and $N(t) \sim t^{-1}$. The present observations, generally on more concentrated solutions of lower molecular weight and in MCH or CH rather than DEO, failed to capture the process at an early enough stage to measure the kinetic order for the development of the ξ_2 structure, except for the experiments reported above for PS/400K-CH, 0.13%, where we also found $\xi_2 \sim t^1$ in agreement with the Japanese workers. On the other hand, we were unable to observe the later stage $\xi_2 \sim t^{1/3}$ process, most likely because sedimentation of the larger polymer-rich particles from MCH or CH solutions is too rapid to permit observation of this later stage process. In a separate set of experiments we attempted deep quenches in DEO solutions but were not successful in reproducing the Japanese results because of technical difficulties.[31]

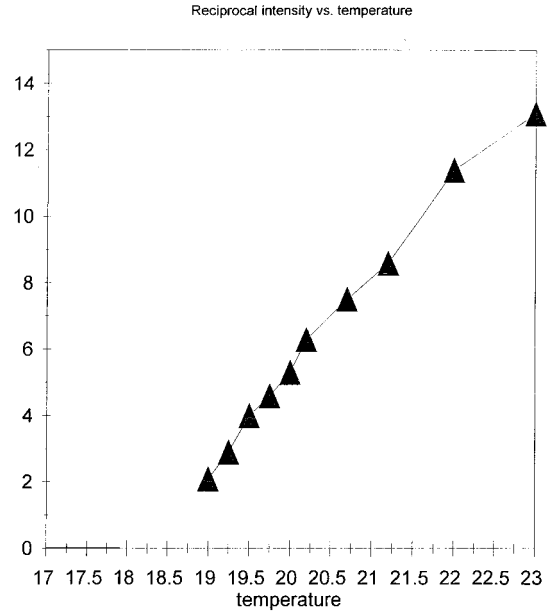

Figure 8. Reciprocal scattering intensity vs T for a PS90K/CH 6.6 wt % solution approaching its cloudpoint. For this solution $T_{cp} = 18.75$ °C and $T_{sp} = 18.3$ °C.

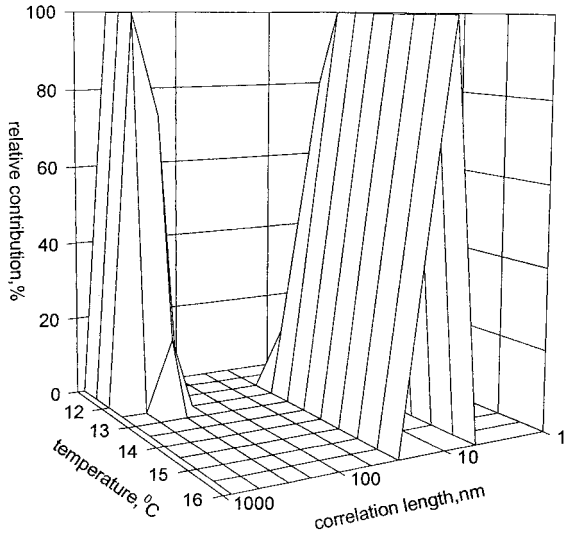

Figure 9. Continuous quench from a PS90K/CH 0.2 wt % solution ($T_{cx} = 14.3$ °C, $T_{cp} = 12.9$ °C, scattering angle (2q) = 30°), 19 °C to 12 °C. The discontinuous splitting to the ξ_1/ξ_2 structure is apparent, as is the growth of the ξ_2 particles, which in the present (low concentration) case remains suspended for the duration of the experiment.

4. Conclusion and Remarks

This paper reported on DLS measurements on dilute PS/cyclohexane and PS/methylcyclohexane solutions at or near precipitation in the nucleation/growth (NG) region. Most noticeably we observe the monomodal single exponential decay pattern characterizing the hydrodynamic correlation length in the parent solution to split discontinuously to a bimodal pattern near the cloudpoint. The new pattern consists of an essentially unchanged small (fast) mode (ξ_1) assigned to the solvated single polymer species, and a much larger (slow) mode (ξ_2) assigned to preprecipitating or precipitating nucleii of polymer rich phase. In the immediate vicinity of the cloudpoint, ξ_2 growth is too fast to follow quantitatively with the present DLS technique, but nonetheless, interesting qualitative or semiquantitative observations are possible. Most important the bimodal pattern dominates throughout. So long as the quench is held above T_{cp} it holds unchanged for times which may exceed hours, but once T is lowered below T_{cp}, precipitating particles develop rapidly and settle from solution. That process involves a certain increase and broadening in the large component of the distribution, but the essential observation—bimodality—holds throughout.

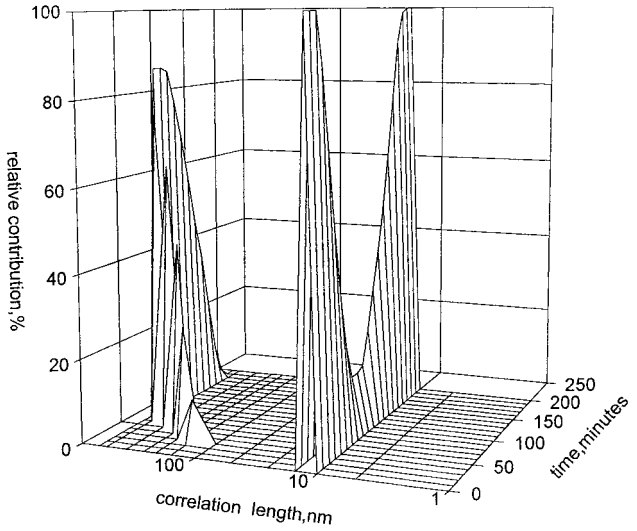

Figure 10. Step quench to a temperature 0.22 K above T_{cp} for a PS400K/CH, 0.13 wt % solution, $2\theta = 30°$. Note the induction time of ~1 h to appearance of the ξ_1/ξ_2 structure. The initial development of ξ_2 and $I(\xi_2)$ is first order (see Figure 11 and Table 2). See text for further discussion, especially in regard to the growth and decay of the ξ_2 structure and the corresponding minimum in $I(\xi_2)$.

Table 2. First-Order Rate Constants, $d\xi_2/dt = k_\xi\xi_2$ and $dI(\xi_2)/dt = k_I I(\xi_2)$ for NG Precipitation from 0.13 wt % PS400K/CH Solutions at Various Quench Depths and Induction Times, t_{ind}

$\delta = T_q - T_{cp}$	$10^2 k_\xi$	$10^2 k_I$	t_{ind}/min
0.05			1
0.07	8.6	9.3	
0.11	1.1	3.5	14
0.14	1.8	1.2	25
0.16	1.5	1.7	35
0.23	1.1	1.3	60
0.27	1.6	1.0	75
0.30	1.1(0.1)[a]	0.3	150
0.34	1.2(0.04)[a]	0.2	230

[a] Parenthesized values refer to long-term rates of change (see lines 7a and 8a, Figure 11c).

By lowering the concentration and minimizing quench depth, one can slow the rate of development of the ξ_2 mode and determine its kinetic order. For shallow quenches observed at low angle (to increase sensitivity) we find early stage ξ_2 and $I(\xi_2)$ to be kinetically first order. That observation is in agreement with literature studies[14] in diethyl oxalate solvent (DEO) where mother and daughter phases are isopycnic so that sedimentation is delayed. Even so, we were not able to look at very late stages of $\xi_{e,2}$ development and cannot comment on reports that late stage kinetic order falls to ~1/3. An intriguing and unexpected aspect of the shallow quench experiments was the observation that an induction time, t_{ind}, is involved with the first appearance of the ξ_2 structure. t_{ind} falls rapidly toward zero with δ ($\delta = T_q - T_{cp}$), but for shallow quenches, it can be as long as several hours. Clearly observations of the kind we

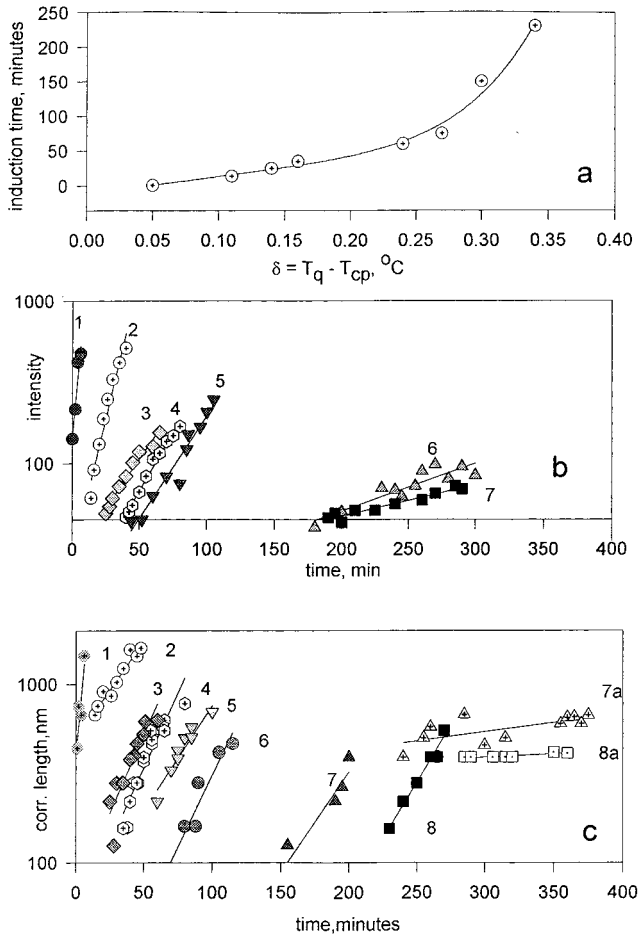

Figure 11. Early stage kinetics of nucleation and growth for precipitation for PS400K/CH, 0.13 wt %, $2\theta = 30°$, $T_{cp} = 22.90$ °C. Each data point in part a or set of data points (parts a and b) depicts results for a quench ending at $T_{cp} + \delta$. Key: (a) induction time vs δ; (b) $\log(I(\xi_2))$ vs time, reading from the left $\delta = 0.07$, 0.11, 0.14, 0.17, 0.23, 0.30, and 0.34 K, (curves 1 to 7), $I(\xi_{e,2})$ is in arbitrary units; (c) $\log(\xi_e/\text{nm})$ reading from left $\delta = 0.07$, 0.11, 0.14, 0.16, 0.24, 0.27, 0.30, and 0.34 K (curves 1 to 8). The lines marked 7a and 8a show the trend in very long time growth in particle size.

report here imply the need for careful and patient sample treatment before interpreting DLS data in the metastable regime in terms of thermodynamic or pseudo-thermodynamic equilibrating distributions of prepre-cipitation or precipitating nucleii. It is also important to keep in mind that DLS ξ_2 (slow mode, large particle) intensity is highly q-dependent because of interference effects. For example, at 90° we were unable to observe DLS ξ_2 splitting for PS30K/MCH above T_{cp}, even though at 15° the ξ_2 pattern developed at temperatures as high as $\delta = 1.35$ K, albeit after a 2 h delay. Such results establish that a long-range ordering process prior to precipitation exists in the metastable NG part of the phase diagram. The phase transition, discontinuous (i.e. bimodal) so far as DLS *structure* is concerned, is kinetically more gradual. We emphasize that remarks in this section apply to the low-concentration NG part of the phase diagram. At higher concentrations, both the rates and the DLS structural patterns characterizing precipitation change as one moves from the NG to the SD/P parts of the phase diagram.

Acknowledgment. This work was supported by the U.S. Department of Energy, Division of Materials Sciences (DE 88ER45374).

References and Notes

(1) Imre, A.; Van Hook, W. A. *J. Phys. Chem. Ref. Data* **1996**, *25*, 637.
(2) Kiepen, F.; Borchard, W. *Macromolecules* **1988**, *21*, 1784.
(3) Luszczyk, M.; Van Hook, W. A. *Macromolecules* **1996**, *29*, 6612.
(4) Ratzsch, M.; Kehlen, H. *Prog. Polym. Sci.* **1989**, *14*, 1.
(5) Jancso, G.; Van Hook, W. A. *Chem. Rev.* **1974**, *74*, 689.
(6) Szydlowski, J.; Van Hook, W. A. *Macromolecues*, **1998**, *31*, xxxx submitted for publication.
(7) Prigogine, I.; Defay, R.; Everett, D. H. (translator): *Chemical Thermodynamics*; Longmans-Green: London, 1954; Chapter 16.
(8) Cummings, A.; Wilthuis, P.; Bates, F. S. *Phys. Rev. Lett.* **1990**, *65*, 863.
(9) Cummings, A.; Wilthuis, P.; Bates, F. S.; Rosedale, J. H. *Phys. Rev. A* **1992**, 45, 885.
(10) Kedrowski, C.; Bates, F. S.; Wilthuis, P. *Macromolecules* **1993**, *26*, 3448.
(11) Stepanek, P.; Lodge, T. P.; Kedrowski, C.; Bates, F. S. *J. Chem. Phys.* **1991**, *94*, 8289.
(12) Zywocinski, A.; Wieczorek, S. A.; Van Hook, W. A. *J. Polym. Sci., Polym. Phys.* **1995**, *33B*, 595.
(13) Tomlins, P. E.; Higgins, J. S. *J. Chem. Phys.* **1989**, *90*, 6691.
(14) Sato, H.; Kuwahara, N.; Kubota, K. *Phys. Rev. E* **1994**, *50*, 303.
(15) Krishnamurthy, S.; Bansil, R. *Phys. Rev. Lett.* **1983**, *50*, 2010.
(16) Tanaka, H. *Phys. Rev. Lett.* **1993**, *71*, 318.
(17) Haas, C. K.; Torkelson, J. M. *Phys. Rev. Lett.* **1995**, *75*, 3134.
(18) Howland, R. G.; Wong, N. C.; Knobler, C. M. *J. Chem. Phys.* **1980**, *73*, 522.
(19) Mayer, W.; Woermann, D. *J. Chem. Phys.* **1990**, *93*, 4349.
(20) Abraham, F. F. *Homogeneous Nucleation Theory*; Academic Press: New York, 1974.
(21) Zettlemoyer, A. C., Ed. *Nucleation*; Marcel Dekker: New York, 1969.
(22) Bowers, P. G.; Bar-Eli, K.; Noyes, R. M. *J. Chem. Soc., Faraday Trans.* **1996**, *92*, 2843.
(23) Pecora, R., Ed. *Dynamic Light Scattering*; Plenum: New York 1985.
(24) Brown, W., Ed. *Dynamic light scattering. The method and some applications*. Oxford Science Publ.: Oxford, England, 1993.
(25) Provencher, S. *Comput. Phys. Comm.* **1982**, *27*, 213.
(26) Brown, W.; Nicolai, T. *Colloid Polym. Sci.* **1990**, *268*, 977.
(27) Schmidt, M. In *Dynamic light scattering. The method and some applications*; Brown, W., Ed.; Oxford Science Publ.: Oxford, England, 1993; Chapter 8.
(28) Kratochvil, P. *Classical light scattering from polymer solutions*; Elsvier Press: Amsterdam, 1987.
(29) Fetters, L. J.; Hadjichristidis, N.; Lindner, J. S.; Mays, J. W. *J. Phys. Chem. Ref. Data* **1994**, *23*, 619.
(30) Weitz, D. A. Pine, D. J. *Dynamic light scattering. The method and some applications*; Brown, W., Ed.; Oxford Science Publ.: Oxford, England, 1993; Chapter 16.
(31) We were unable to make low-angle DLS measurements of acceptable quality in DEO solutions. The reason, we think, is that DEO is very hygroscopic and the adsorbed water hydolyzes to produce oxalic acid, an insoluble precipitate that acts like dust in the sample, ruining it for high-quality DLS measurements.

MA971776W